Microfluidics investigation of the effect of bulk nanobubbles on surfactant-stabilised foams

Leslie Labarre, Arnaud Saint-Jalmes, Daniele Vigolo

Microfluidics investigation of the effect of bulk nanobubbles on surfactant-stabilised foams

L. A. Labarre[1], A. Saint-Jalmes[2], D. Vigolo[1,3,4,]*

(1) School of Chemical Engineering, University of Birmingham, Birmingham, B15 2TT, UK.

(2) Univ Rennes, CNRS, IPR (Institut de Physique de Rennes) - UMR 6251, F-35000 Rennes, France

(3) The University of Sydney, School of Biomedical Engineering, Sydney, NSW 2006, Australia

(4) The University of Sydney Nano Institute, University of Sydney, Sydney, NSW 2006, Australia

* daniele.vigolo@sydney.edu.au

KEYWORDS foam, nanobubbles, stability, microfluidics.

ABSTRACT

In aqueous foams, the bubble size usually spans from tens of microns to centimetres. However, it is possible to create much smaller and stable bubbles in solutions: nanobubbles have diameters well below a micron. Many issues are still pending on nanobubbles, especially regarding their stability. Here, we address if and how the addition of nanobubbles may change the interfacial and foaming properties of surfactant solutions. Using a first microfluidic device, nanobubbles are formed within the aqueous surfactant solutions (SDS and Triton X-100 at different concentrations). A second microfluidic device then generates foams from these solutions. Additionally, we report systematic results on the interfacial and bulk properties of such solutions. Finally, we show that nanobubbles have some effects on almost all the measured quantities; however, the most striking one is enhancing the foaming of the solutions with an initial poor foamability. These measurements provide us with a comprehensive set of new results allowing us to draw a first multi-scale picture of how far nanobubbles could potentially act as foam boosters and stabilizers or be implemented in colloidal formulations. Yet, more investigations are required to unravel the mechanisms leading to our results.

1/ INTRODUCTION

Stability is a crucial issue for many industrial processes involving aqueous foams. Three destabilising events primarily determine foam evolution: drainage, coarsening, and coalescence [1,2]. To prevent those events to occur, surfactants [3], nanoparticles [4,5], polymers [6], or a combination of the above [7] can be employed. Despite the development and improvement of such combination, this is not always enough to ensure the optimal foam stability necessary for each specific application. For example, in enhanced oil recovery [8–10], foams are exposed to high-temperature and high-pressure conditions that make foam stability challenging.

One of the main goals of current foam formulation engineering is to reduce the environmental impact by decreasing the amount of surface-active agents or by replacing them with biocompatible and biodegradable surface active-agents. For example, scientists have exploited bio-based and biocompatible products such as chitosan [11,12] to generate and stabilise foams. Nevertheless, the extraction and processing of these products remain costly.

In this work, the feasibility of employing very small and stable objects, called nanobubbles, was studied. In the last two decades, such nanobubbles were discovered and investigated [13–15]. There are two kinds of nanobubbles: surface nanobubbles, defined as gas-filled spherical caps of 10 to 100 nm height and a contact line radius between 50 to 500 nm present on hydrophobic surfaces, and bulk nanobubbles, described as gas-filled spherical bubbles with a diameter below 1 micron located in the bulk of an aqueous solution [16]. In this study, the focus is given to bulk nanobubbles.

Because of their extraordinary stability, these bubbles have been introduced and employed in a wide range of applications, from surface cleaning [17,18] to froth flotation [19,20]. This super stability is not fully understood, but the leading theories considered the bubble surface charge

density [21] as the determining factor for their stability. Indeed, the ion-stabilisation model [22] explains the single nanobubble stability by the existence of an electrostatic pressure that balances the high internal Laplace pressure. Additionally, the DLVO theory successfully describes the dependence of bulk nanobubbles cluster stability on parameters such as pH and electrolytes in solution [21]. Two studies conducted by Ushida *et al.* and later Yesui *et al.* showed that the presence of nanobubbles in solution could affect various gas-liquid interfacial properties [23] [24]. The important role of nanobubbles on the stability of nanoparticle dispersions was also demonstrated. Zhang and Seddon highlighted potential nucleation or attachment of nanobubbles onto negatively charged gold nanoparticles above a threshold nanoparticle size [25]. Zhang et al. found that the ratio of nanoparticle to nanobubbles in solution could be used to tune the zeta potential of the resulting dispersion of initially positively charged Polystyrene latex nanoparticles [26]. Another recent work was dedicated to studying the combination of nanobubbles with various frothers and hydrophobic nanoparticles and their impact on the separation efficiency in the froth flotation process [20,27–30]. Sobhy and Tao found, for the first time, that froth stability was improved by nanobubbles in the presence of strongly hydrophobic particles [28]. Thus far, few studies have been undertaken to determine if these nanobubbles could affect dispersed colloidal systems such as foams or emulsions.

Therefore, this work investigates for the first time how nanobubbles generated by microfluidics in a well-controlled and reproducible way could affect the properties of foams generated from aqueous surfactant solutions (also produced by microfluidics). In each foam study case, the nanobubble-surfactant solution properties and the resulting foam properties are analysed and compared to the properties of the foam stabilised by surfactant only.

First, the materials and methods employed in this work are described. The results – obtained for two different surfactants and at various concentrations – are then discussed at each relevant length scale for foams: from the microscopic scale of the gas-liquid interface to the bubble scale in bulk and up to the foam itself.

2/ MATERIALS & METHODS

2.a Materials

Two surfactants were studied: Sodium Dodecylsulfate (SDS), an anionic surfactant, and 2-[4-(2,4,4-trimethylpentan-2-yl)phenoxy]ethanol named Triton X-100 (TX100), a non-ionic surfactant. SDS (AR > 99%) and TX100, laboratory grade were purchased from Sigma-Aldrich. All the foaming solutions were prepared by mixing the surfactant in Millipore water (18.2 mS m^{-1} conductivity) with a magnetic stirrer at 25°C to achieve complete dissolution. All the stock solutions were filtered with a 0.2 µm Acrodisc syringe filter. These two surfactants were investigated at four concentrations: 0.5, 1, 2.5 and 5 times their critical micellar concentration (cmc). The cmcs were found in the literature at 6.0 x 10^{-4} mol L^{-1} - for TX100 and 8.3 x 10^{-3} mol L^{-1} for SDS at 25°C [31–33]. It should be noted that TX100 has a cmc more than ten times smaller than SDS.

2.b Bulk nanobubble generation via microfluidics

This study employed two types of microfluidic devices: a single-depth microfluidic device for foam generation and a two-depth microfluidic device for nanobubble generation from surfactant solution. The silicon mould used to make the two-depth microfluidic device was purchased externally from the Nanofabrication Centre (Southampton, UK).

All the microfluidic devices were fabricated in Polydimethylsiloxane (PDMS, Sylgard™ 184 Silicone Elastomer Kit, Dow Chemical) by soft lithography [34,35]. The PDMS devices were then irreversibly bonded to a microscope glass slide by corona discharge [36]. To ensure a homogeneous bubble formation in the channel [37], the devices were surface treated to become hydrophilic with a layer-by-layer technique by flowing alternated segments of prop-2-en-1-amine;hydrochloride (PAH, Sigma Aldrich) and 4-ethenylbenzenesulfonic acid (PSS, Sigma Aldrich) solutions (both 0.1% w/v in 0.5 M aqueous sodium chloride, NaCl solution) with aqueous NaCl washing solution (0.1 M) segments in between as described in [38].

The two-depth microfluidic device used for nanobubble generation was similar to the one described in Evans *et al.* [39,40]. It was made of PDMS and consisted of two regions with different depths (d_1 = 25 µm and d_2 = 55 µm): the shallow zone contained a flow-focusing junction where the 50 µm wide gas inlet met with two 100 µm wide liquid inlets. The channel then suddenly expanded in both width, from the nozzle, w_n = 20 µm up to w_3 = 280 µm in the expansion channel, and depth, as depicted in Figure 1. For the purpose of this study, a fixed nozzle position and nozzle diameter were kept constant throughout the whole experiment to ensure steady and reliable experimental conditions. The foam was generated with a second microfluidic device with similar dimensions but without a change of depth.

One reservoir of air was connected via a pressure controller (OB1 MK3, Elveflow) to the gas inlet via 0.020" x 0.060" OD Tygon microbore tubing (Cole-Parmer Instrument Co. Ltd., UK) to accurately control the gas inlet pressure. A 10 mL syringe filled with the sample was connected to the liquid inlet via the same tubing, and its flow rate was finely controlled with a syringe pump (Harvard Syringe Pump 11 Pico Plus Elite, Harvard apparatus). The liquid flow rate was set at 90 µL min^{-1} and the gas inlet pressure was fixed at 1000 mbar. The microfluidic device used for the generation of nanobubbles was cleaned thoroughly by flowing pure water at 90 µL min^{-1} for 10

min prior to any experiment. A 1 mL nanobubble sample was collected into a disposable plastic cuvette or into a clean and dry glass beaker at the channel exit.

One of this design's main peculiarities is the depth change between the nozzle and the expansion channel. To produce an atomization-like spray, the depth was more than doubled (from d_1 = 25 µm to d_2 = 55 µm) so that the pressure drop was abruptly changed [39,40]. The reduction in pressure led to hydrodynamic cavitation and to the bulk nanobubbles generation. The nanobubbles concentration after one generation cycle was assumed to be about 10^9 bubble mL^{-1} based on the similar experimental conditions (device geometry, flow rate and pressure) employed by Evans et al. [39,40].

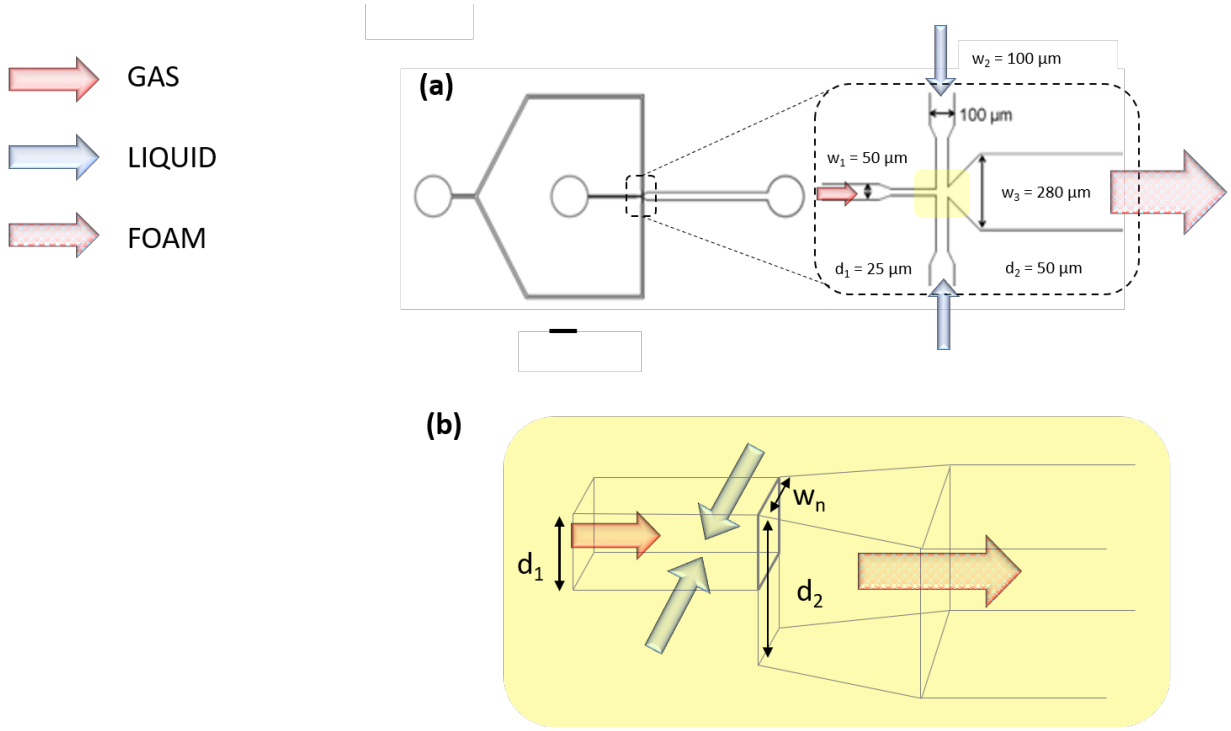

Figure 1 (a) schematic of the two-depth (d_1 = 25 µm & d_2 = 55 µm) flow-focusing device (left) and a zoomed in view of the two-depth flow focusing junction (right) for bulk nanobubbles generation. Scale bar = 1000 µm. (b) In yellow, a schematic representation of the cross-sectional view of flow-focusing two-depth device employed for bulk nanobubbles generation with w_n = 20 µm.

2.c Interfacial & bulk characterisation

The presence of nanobubbles and their size distribution in pure water and in surfactant solutions were analysed at 25°C by dynamic light scattering (DLS, Zetasizer NanoZSP, Malvern Instruments Ltd) before and after the microfluidic foaming of the resulting solutions.

The zeta potential of the various nanobubble solutions was measured using a Zetasizer NanoZSP (Malvern instruments Ltd). This measurement was done before and after the foaming of the solutions. In the latter case, the foam was left to drain and the resulting liquid was collected and analysed for each condition.

The temporal evolution of the surface tension at short timescales (down to 1 ms) of the surfactant solutions was also analysed with a maximum bubble pressure tensiometer (Sinterface BPA-1). This method allows for the measurement of the maximum pressure that needs to be applied to create and detach a bubble at the tip of a 0.13 mm diameter capillary placed vertically in a liquid [41].

2.d Foam generation & analysis

A foam was generated by co-injection of a foaming solution and air in a 25 µm depth flow-focusing device. The gas and liquid inlet pressures were controlled by a pressure controller and set at 1000 mbar and 1900 mbar, respectively. The foam was formed and studied downstream in the 280 µm wide channel. The foam was then collected into a glass cuvette (0.4 x 0.8 mm), previously cleaned with water and ethanol and dried with air, via a 15 cm length tubing, 0.020" x 0.060" OD Tygon microbore tubing (Cole-Parmer Instrument Co. Ltd., UK). The foaming time was fixed at 1 minute after the first bubble exited the tubing and entered the glass cuvette.

In this work, the foamability was evaluated by the initial foam heights (Figure 1), initial liquid fractions (Figure 1) and qualitatively by microscopy observations (Figure 1). For the latter, a

small amount of foam, taken at the early stage of its life, was deposited on a glass slide and covered with a cover slip.

The height evolution of the foam was measured manually by following the foam column height over time. The foam height was normalised by the value obtained after 1 min (end of the foaming process) to study its evolution. The liquid fraction was evaluated by weighting the amount of liquid left in the cuvette (m_L) once the foam had drained. The initial uniform foam liquid fraction (φ_L) was computed from the following expression:

[1]

where, h_{foam} is the initial foam height, A_{cuv}, the cross-section of the measuring cylinder and ρ_L, the volumetric mass density of the foaming liquid.

3/ RESULTS ON INTERFACIAL PROPERTIES OF SURFACTANT SOLUTIONS

Here, we present results obtained at the scale of the liquid-gas interfaces, to determine the possible impact of the presence of nanobubbles. First, the short timescale tensiometry results are presented in Figure 1.

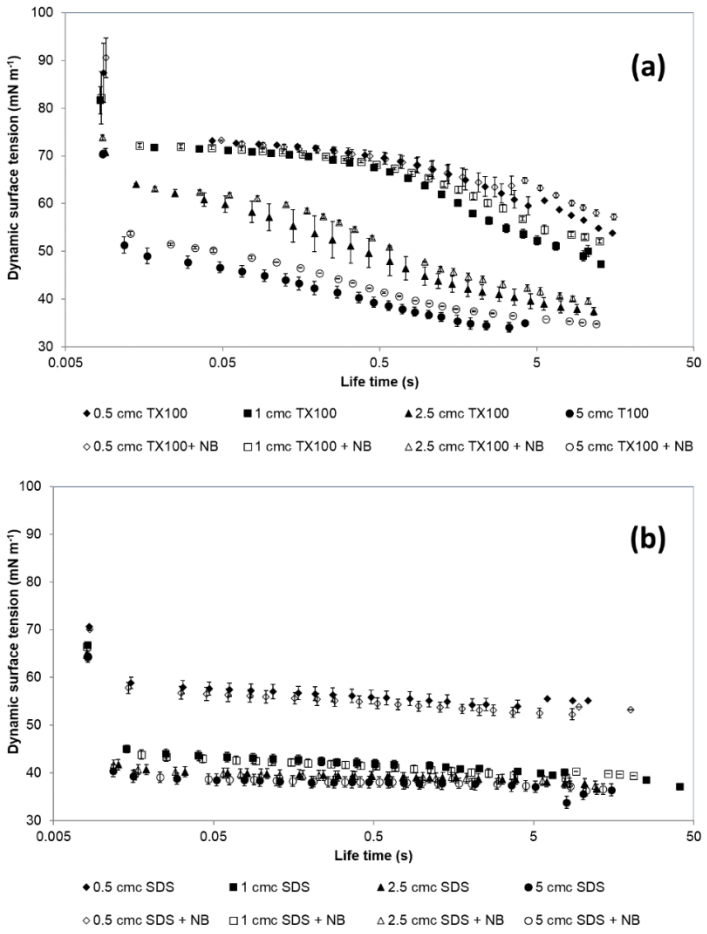

Figure 1 Dynamic Surface Tension results for the set of TX100 (a) and SDS (b) solutions from 0.5 (♦,◊), 1 (■,□), 2.5 (▲,Δ and 5 cmc (●,○) described by filled symbols for surfactant solutions and by unfilled symbols for nanobubble-surfactant solutions. The error bars are standard errors.

Overall, the results for the pure surfactant solutions were consistent with the literature. The difference between TX100 and SDS solutions resided in the dynamics of adsorption. Indeed, the most important aspect is the characteristic adsorption time that depends on the diffusion coefficient of the surfactant and also quadratically on the concentration [42]. As TX100 and SDS have different cmcs, their absolute concentrations are different at constant cmc units, as in our case. Consequently, SDS molecules, while diffusing at an interface, cover it faster than TX100 molecules. The equilibrium is only reached in a few seconds for TX100 solutions (even above the cmc), while equilibrium is quasi-instantaneous for SDS solutions at all concentrations.

It is important to point out that the choice of surfactant and concentrations in this study allowed to span over the full range of possible interfacial dynamics. At a typical timescale of 1s – the time required for producing a bubble in the foaming device – these results show that the following foaming experiments are performed from almost bare interfaces (for the lowest TX100 concentrations) up to fully saturated interfaces (for the highest concentrations of SDS).

Qualitatively, the impact of nanobubbles (NBs) on the interfacial properties was mainly noticed for the solutions of TX100: the surface tension of the nanobubble-TX100 solutions was always slightly greater than the reference (at the longest timescales at low concentrations and throughout the whole dynamical as the concentration gets to 5 cmc). However, this effect remained small. Oppositely, for SDS solutions, the presence of nanobubbles did not impact the dynamic surface tension. To quantitatively evaluate the differences between the NBs and non-NBs solutions, an ANOVA statistical analysis was performed to evaluate the impact of nanobubbles on the surface tension measurement over the whole spectrum of bubble life time per surfactant concentration and surfactant type presented in Figure 1. The results are summarised in **Table S1** in the Supplementary Material section. Despite the results of the ANOVA test showing that there was no significant difference (p-value > 0.05) caused by the presence of nanobubbles for the whole range of surfactant concentration, the p-values for TX100 are clearly smaller than for SDS except at 0.5 cmc, showing that the NBs have more impact on TX100 than on SDS interfacial properties.

4/ RESULTS ON BULK PROPERTIES OF NBS-SURFACTANT SOLUTIONS

To complete the analysis of the potential multi-scale impact of nanobubbles on this system, we characterized them in the bulk, once dispersed in the surfactant solutions. More importantly, this study allows us to compare the features of the population of nanobubbles in different surfactant solutions before these solutions are foamed and after their foaming.

4.a Gaseous nature of bulk nanobubbles in pure water

The nature of the nano-entities generated from pure water by the 20 µm nozzle two-depth microfluidic device was verified to be nanobubbles. Following what was discussed by Nilmalkar *et al.*, the gaseous nature of bulk nanobubbles was simply demonstrated by freezing a vial containing an aqueous solution of bulk nanobubbles generated by microfluidics, by dipping it for 30s in liquid nitrogen and by thawing it at room temperature for a whole day [43]. After this step, no nanobubbles were detected via DLS. This result demonstrated that nanobubbles were made of gas as solid impurities would have otherwise remained in solution and eventually agglomerated after thawing.

4.b Nanobubble-surfactant dispersions

The nanobubble size distributions in the presence of surfactant are given in Figure 1 for the different concentrations investigated (denoted “NB”). For comparison, equivalent distributions after the microfluidic foaming process (denoted “NB foamed”) were obtained from the analysis of the foam drained liquid and are also reported in Figure 1. It was observed that the foaming process did not significantly affect the nanobubble-surfactant distributions as the sizes were similar throughout the different concentrations before and after foaming (see ANOVA statistical analysis in the **Table S2** in the Supplementary Material section). Therefore, this shows that the foaming of a surfactant solution containing nanobubble, together with a subsequent foam drainage, are not processes able to modify the amount of nanobubbles and their size distribution. Yet, an exception was visible at a SDS concentration of 0.5 cmc: the foaming process caused a

strong increase in the nanobubble average size, and this effect remains to be investigated in more detail.

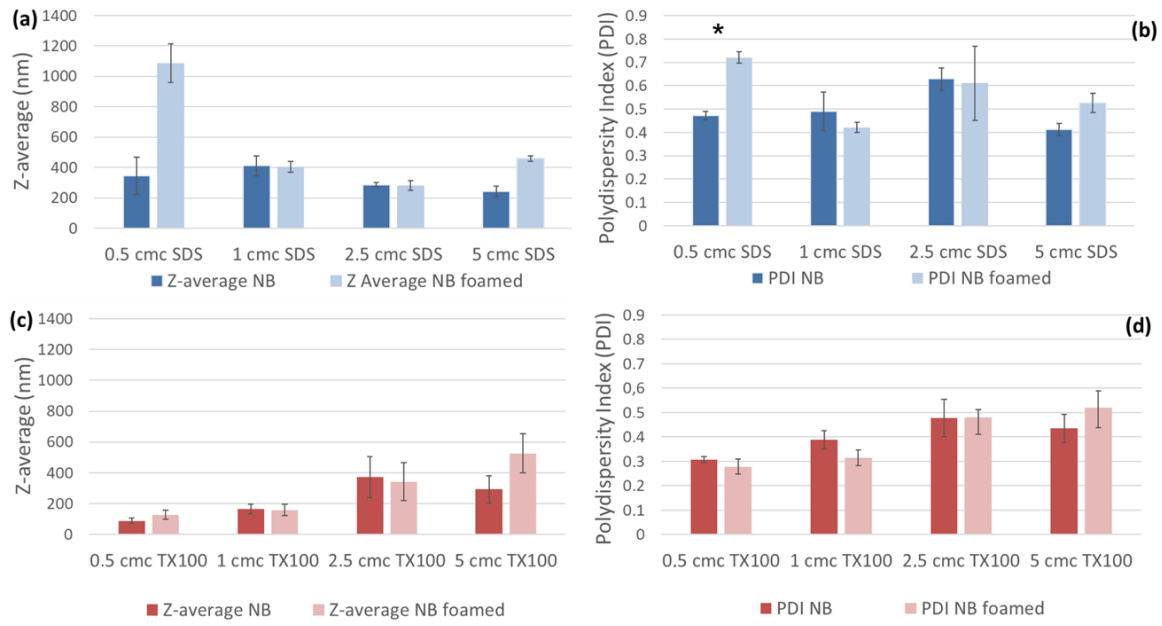

Figure 1 Z-average diameter (a,c) & Polydispersity (b,d) evolutions for the nanobubble-surfactant dispersions before and after foaming for the four SDS and Triton X-100 surfactant concentrations. The error bars are standard errors. Based on the ANOVA test, the asterisk * describes a p-value below 0.05.

4.c Zeta potential

The evolution of the zeta potentials of the surfactant solutions containing NB is reported in Figure 1. Here again, the results were studied before and after the foaming/drainage processes, for the two surfactants and different concentrations.

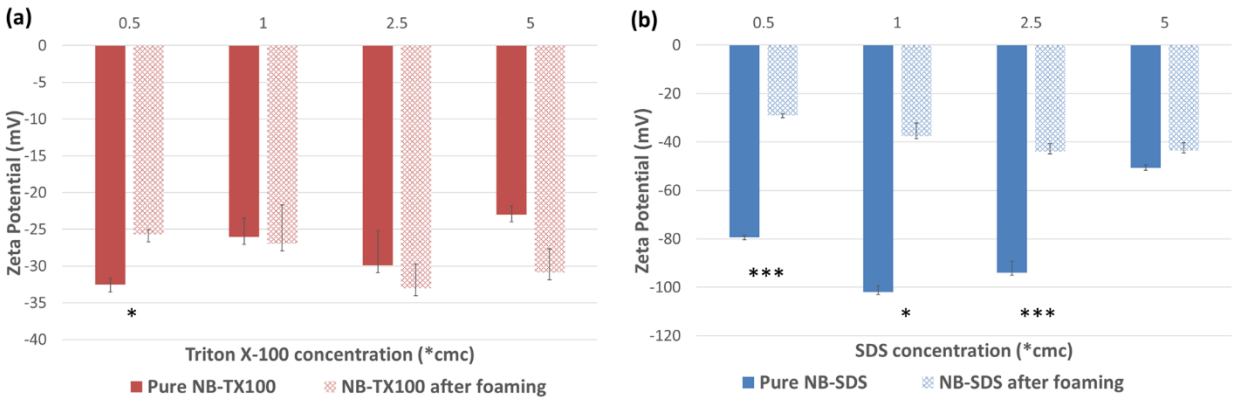

Figure 1 Zeta potential evolution of the nanobubble-surfactant dispersions in water for various Triton X-100 (a) and SDS (b) concentrations (0.5, 1, 2.5 and 5 cmc) before (dark red and blue) and after foaming (light red and blue). The error bars are standard errors. Based on the ANOVA test, the asterix * describes a p-value below 0.05, ** means a p-value below 0.005 and *** p-value below 0.0005, respectively.

The results of the ANOVA statistical analysis on the effect of foaming and surfactant concentration on the nanobubble population are summarised in **Table S3** in the Supplementary Material section. For TX100, the results show that the effects of the foaming process and the concentrations on the Zeta potentials are always small, with only some statistically significant impact at 0.5 cmc TX100, consistent with the non-ionic nature of the surfactant. Oppositely, for the ionic SDS surfactant, both surfactant concentration and the foaming process significantly impacted the zeta potential. Note first that the sizeable negative zeta potentials found from 0.5 to 2.5 cmc were consistent with those reported in the literature for the combination of SDS and nanobubbles generated via ultrasonic cavitation [44]. Based on this paper, SDS was said to enhance the nanobubble charge density in the solution. Indeed, Nirmalkar et al. (2018) and, very recently Lee and Kim (2022), agreed upon the positive effect of SDS on nanobubble charge density and subsequent increase in stability.[44,45] More specifically, Lee J. and Kim J. (2022) observed that nanobubble concentration made by ultrasonication dramatically increased with the SDS concentration.[45] They suggested that as the SDS concentration in the solution was increased, nucleation occurred because of the influence of SDS molecules that adsorbed to the gas–liquid of the bubbles. In addition, the bubbles generated in the SDS solution presented a

strong negative zeta potential, and thus, a strong repulsive force occurred between adjacent bubbles, enhancing their stability.

In parallel, a strong effect of the foaming/drainage process on the nanobubble-SDS dispersions zeta potential was monitored (see p-values in **Table S3**). While the results on the NB sizes (Figure 1) showed the high stability of the solutions against foaming/drainage, these complementary results indicated that – at least for an anionic surfactant like SDS – the foaming/drainage sequence was not as inert as expected, and could induce some complex charge re-organization leading to zeta potential values divided by two as seen in Figure 1.

5/ RESULTS ON FOAMS

Previous sections were dedicated to the impact of NB in bulk and at interfaces. Building on these first elements, we complement our multi-scale study by presenting the results at the foam macroscopic scale.

5.a Foamability

In this section, the foamability was evaluated by the initial foam heights (Figure 1), initial liquid fractions (Figure 1) and qualitatively by microscopy observations (Figure 1).

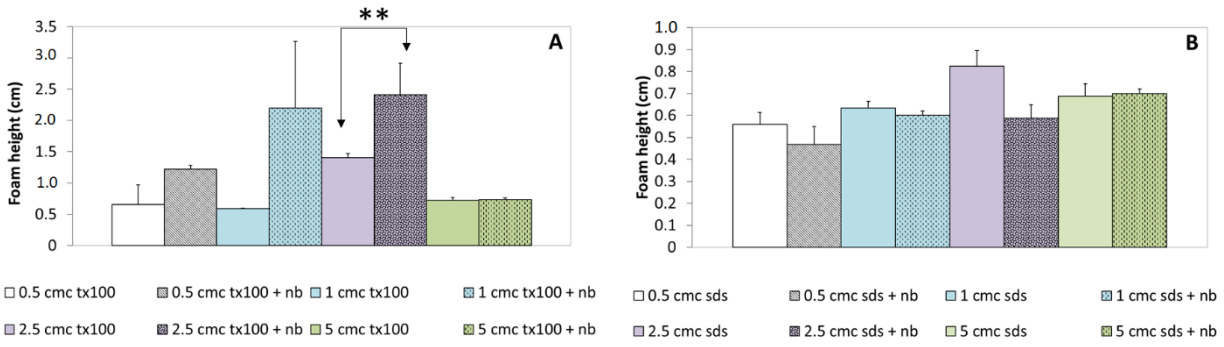

Figure 1 Initial foam heights after 1-minute foaming for 0.5 (white), 1 (blue), 2.5 (purple) and 5 (green) cmc Triton X-100 (A) and SDS solutions (B) (blank) versus bulk nanobubbles + Triton X-100 and SDS solutions respectively (symbols). The error bars are standard errors. Based on the ANOVA test, the asterisk " ** " means a p-value below 0.005.

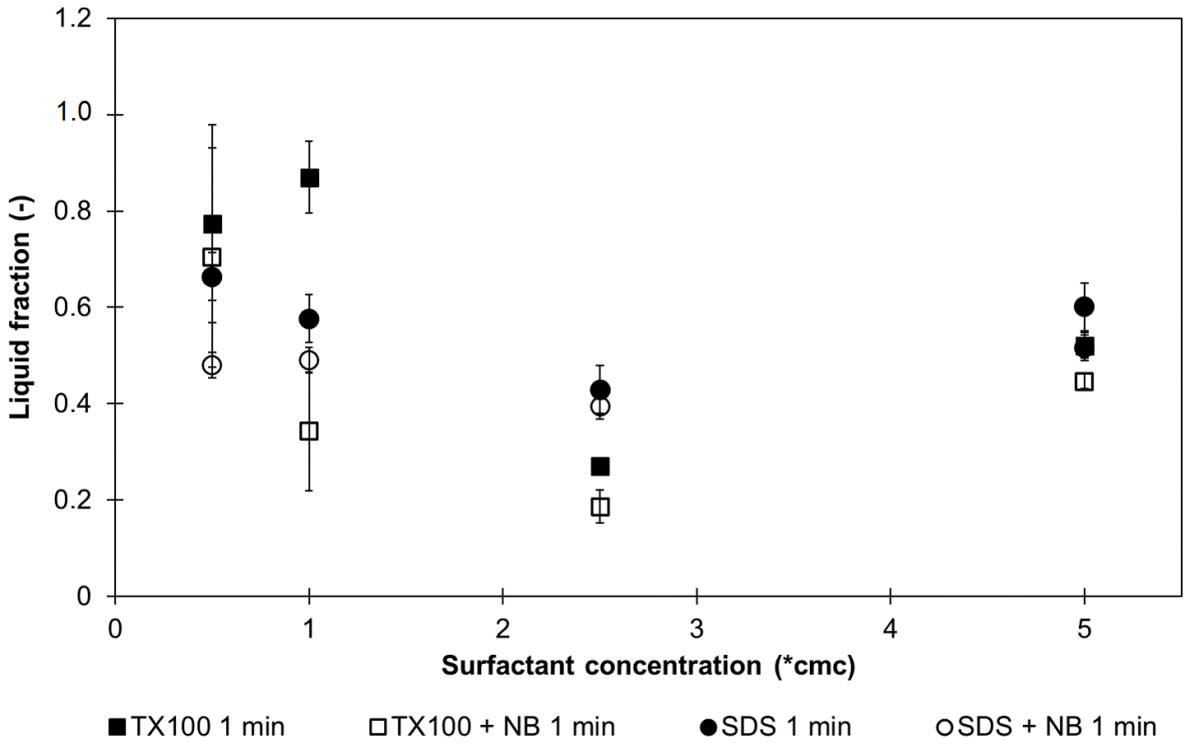

Figure 1 Foam liquid fraction evolution for Triton X-100 (square) and SDS solutions (circle) (filled symbols) versus bulk nanobubbles + Triton X-100 and bulk nanobubbles + SDS solutions (unfilled symbols). The error bars are standard errors.

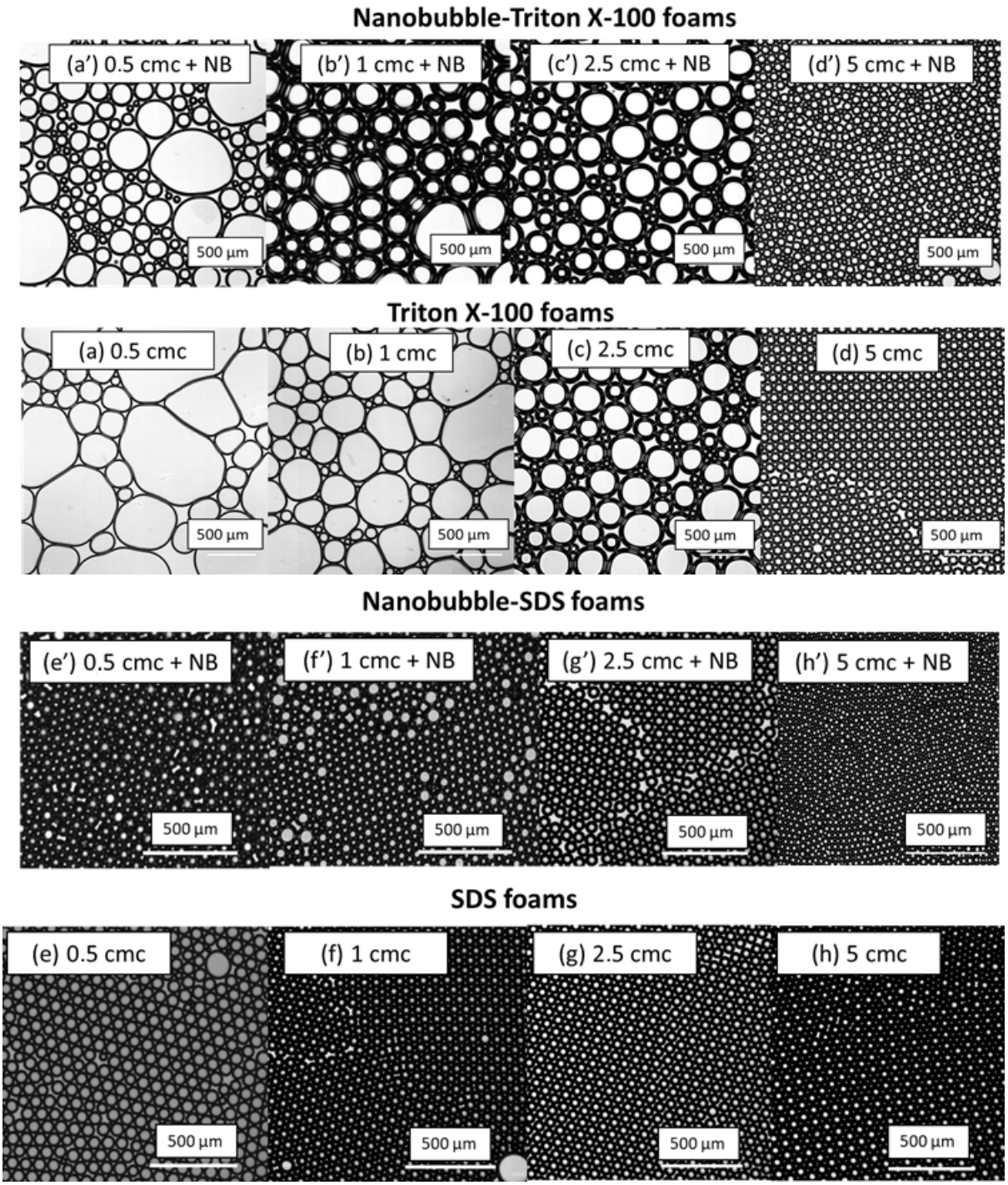

Figure 1 Foams after 5s deposition on a glass slide under a cover slip for various concentrations of Triton X-100 (0.5 (a), 1 (b), 2.5 (c), 5 (d)) cmc solutions & Triton X-100 – nanobubble solutions at 0.5 (a'), 1 (b'), 2.5 (c') and 5 cmc (d') and of SDS (0.5 (e), 1 (f), 2.5 (g), 5 (h)) cmc solutions & SDS – nanobubble solutions at 0.5 (e'), 1 (f'), 2.5 (g') and 5 cmc (h').

5.1.a. SDS: Optimum foaming conditions with & without NB

In this section, the foamability of SDS solutions with and without nanobubbles was analysed. First, it was noted that the device produced "wet" foams, as the liquid fractions were always about 0.5. Consequently, all the SDS foam pictures showed closed, but not packed, spherical bubbles. From Figure 1, the foam height after 1 min appeared almost constant, independent from the concentration and the presence of NB. Consistently, the ANOVA results reported in **Table S4** in the Supplementary Material section confirmed that the surfactant concentration did not impact significantly the foam height and the liquid fraction for the SDS and the SDS-NB solutions. Furthermore, the ANOVA analysis showed that the NB had no, or only a small impact on the foaming of SDS solutions. Besides, the initial microbubble sizes were almost all equal (45 ± 5 µm) as depicted in Figure 1. Thus, all SDS-NB solutions produced optimum foam properties via a controlled microfluidic foaming process, even at the lowest concentrations. Hence, the NB did not impact the foaming efficiency. At this stage, it was interesting to confront these practical observations to the theoretical estimation of the amount of surfactant captured either by the nanobubbles or by the foam microbubbles.

The following expression was used to assess the number of surfactant molecules, N_s, of area A_S employed to cover a bubble surface of radius R_B [24]:

[2]

The surface to cover comprised the total amount of nanobubbles in the liquid contained within the foam and an additional surface from the microbubbles once the solution containing the nanobubbles was foamed. The area per surfactant molecule is 50 $Å^2$ for SDS [46,47]. The number of nanobubbles for 1 m^3 was set at 10^{15} nanobubbles. The nanobubbles diameters employed for the calculation were taken from Figure 1. The microbubbles diameters were estimated from the image analysis of a series of snapshots like the one in Figure 1. In this calculation, an irreversible surfactant adsorption on nanobubble/microbubble surface was considered to simplify the estimation. The detailed figures are available in **Table S7 and Table S8** in the Supplementary Material section.

With these estimations, the required number of surfactants to cover NB (**row E in Table S7 and S8**) turns out to be always *orders of magnitude smaller* than what is required to cover the MB (**row D in Table S7 and S8**). Similarly, there are always enough SDS molecules to cover all the MB, even at the lowest surfactant concentration (**Table S7, row G > row F**).

Thus, these estimations are consistent with the optimal foaming ability measured for the SDS and SDS-NB solutions and with the fact that the NB did not impact the foaming efficiency.

5.1.b. TX100 foams: smooth transition from poor to good foaming

In the following, the foamability of TX100 solutions with and without nanobubbles was studied.

At 0.5 cmc TX100, a very poor foamability was obtained: the liquid fraction was high (> 0.7), resulting from a low gas incorporation corresponding to a 'bubbly liquid' rather than a foam. In consequence, it was nearly impossible to perform relevant microscopic observations of the produced bubbly liquid: the bubbles coalesced very fast, as the liquid drained out rapidly. Instead

- as shown in Figure 1 (a) - only a small number of large coalesced bubbles remained after deposition. Therefore, such pictures were not representative of the produced bubbly liquids.
At 1 cmc TX100, similar unstable foam behaviour was observed despite slightly more foam produced. The foaming properties improved significantly at 2.5 cmc TX100: the foam height doubled with respect to 1 cmc TX100, and the liquid fraction decreased considerably from 0.8 to 0.3, representative of the creation of a foam. On the opposite, at 5 cmc TX100, the foam showed optimum foaming properties and recovered an SDS-like behaviour.

This latter set of results validated the controlled conditions of the experiment and analysis: each system (SDS or TX100) showed similar properties (liquid fraction, height, structure) once the concentrations were well above the cmc.

Thus, from 0.5 to 5 cmc, pure TX100 solutions exhibited a smooth transition from poor to good foaming. Figure 1 (a-d) showed – oppositely to SDS (Figure 8 e-h) – how the foam quality increased with the concentration. At intermediate concentration (2.5 cmc), the foam height was the highest: this result might appear inconsistent with the former observation that the foamability of TX100 is optimum and equal to the one of SDS, only at 5 cmc. However, such foam height comparison should only be performed *at equivalent bubble size and distribution*. In fact, the foam viscosity increases strongly as the bubble size decreases. In the setup, *the pressure was controlled, but not the flow rate*. Therefore, as bubbles got smaller, a higher pressure would have been required to maintain constant the flow rate pushing the foam through and out of the device. Here, the pressure was kept constant; therefore, the flow rate decreased – and so as the total foam height being generated in one minute.

At *0.5 cmc of TX100-NB*, the foamability stayed poor, illustrated by the high liquid fraction of 0.75, and the pictures in Figure 1 (a') only show a few remaining bubbles, after fast coalescence and drainage. Yet, the foamability of the TX100-NB compared to TX100 solution was enhanced (Figure 1). At *1 cmc TX100-NB*, the presence of nanobubbles increased the foam height compared to the 1 cmc TX100 foam despite a slight reduction in bubble size. Figure 8 (b') demonstrate that with the presence of NB in solution, the structure of a foam was obtained. Consequently, the liquid fraction was much lower for the TX100-NB foam, and the "NB-doped" solution incorporated gas more efficiently. At 2.5 cmc, the TX100-NB solution presented a higher foamability for a similar range of bubble sizes (Figure 8 (c) for TX100 & (c') for TX100-NB). At 5 cmc TX100 foams with or without NB displayed the same heights, foam structures and liquid fractions representative of optimum foaming properties. The strong decrease in foam height from 2.5 to 5 cmc for both foams was again explained by the increase in foam viscosity linked to the decrease of the microbubble diameters.

One of the more significant findings to emerge from this study is that in the presence of NB, a similar transition - from poor to optimal foaming - was observed, but *was shifted towards lower concentrations of TX-100*. Taken together, these results suggest that nanobubbles helped the foaming process in the range of concentration where the foaming was poor (0.5, 1 and 2.5 cmc TX100). An implication of this is the possibility that NBs played a "foam booster" role in the poor-to-good (P/G) transition range.

To complement those observations, the nanobubbles' effect per concentration and the impact of the TX100 concentration on the foam height and liquid fraction was evaluated by ANOVA statistical analysis (**Table S5)**. This analysis confirmed the trend observed qualitatively and

notably that the effect of nanobubbles on the foam height distribution of TX100 foams was the strongest at 2.5 cmc.

The analysis also highlighted the fact that the concentration significantly impacted the evolution of the foam height for the pure TX100 solution ($p<0.005$) but the addition of nanobubbles caused the surfactant concentration to have a smaller impact on the foaming properties. Here, the foaming boosting effect of NB counterbalanced the negative effect of the surfactant concentration on the foaming properties. This change is an indicator of the foam "boosting" effect of nanobubbles on the whole range of TX100 concentrations as the foaming properties become less dependent upon the surfactant concentration due to the presence of nanobubbles in the solution.

As previously, these experimental observations were compared to the theoretical estimation of the relative number of surfactants captured by the NB and the microbubbles (MB). As for SDS, Eq. 2 was employed to determine the number of TX100 surfactant molecules required to cover NB and MB. Here, the area per TX100 molecule is close to the one of a SDS molecule, but the cmc of TX100 is 35 times smaller than the one of SDS. Consequently, at the lowest concentration of 0.5 cmc, the total number of TX100 molecules becomes comparable to or lower than the total number of TX100 molecules required for covering all the MB (**Table S8**).

As for SDS, the required number of surfactant molecules to cover the NB (row D in Table S7 and S8) is still orders of magnitude smaller than what is needed to cover the MB (row E in Table S7 and S8). Consequently, in terms of surfactant capturing, the presence of nanobubbles can always be neglected for our experimental conditions. Thus, despite those rough approximations, these estimations show that the poor foaming of TX100 at low concentrations is due to the low value of the cmc, meaning a low number of total surfactant molecules in solution (together with

adsorption dynamics, as shown in Figure 1) and not due to the capture of surfactant molecules by NB.

5.b Foam stability: time evolution

The foam evolution over time was quantified by comparing the normalised foam height evolution reached after 10 min as described in Figure 1.

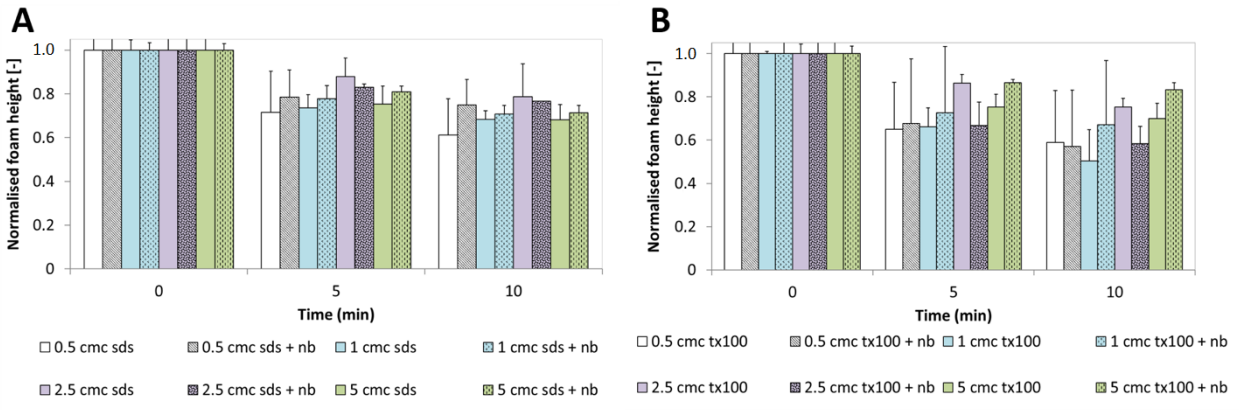

Figure 1 Normalised foam height evolution at 5 and 10 minutes after foaming for 0.5 (white), 1 (blue), 2.5 (purple) and 5 (green) cmc SDS (A) and TX100 solutions (B) (solid colour) versus bulk nanobubbles + Triton X-100 and SDS solutions respectively (coloured lattice). The error bars represent standard error.

Foams made of TX100 were generally more unstable than the SDS foams: on average, the height was halved in 15 minutes, while it was still 2/3 of the initial foam height for SDS after 20 minutes. This showed that drainage and coalescence occurred within these foams.

An ANOVA statistical analysis was firstly used to determine the impact of the presence of nanobubbles on the normalised foam height after 10 minutes for each surfactant concentration. The same method was employed to assess the impact of surfactant concentration on the foam stability, symbolised by the evolution of the normalised foam height after 10 minutes.

The p-values are gathered in **Table S6** in the Supplementary Materials section. Based on those p-values, it was concluded that both the surfactant concentration and the presence of nanobubbles

in SDS solutions did not significantly affect the foam evolution 10 minutes after its generation by microfluidics.

The surfactant concentration impacted significantly the foam height evolution after 10 minutes for TX100 foams ($p = 5.0 \times 10^{-3}$). Oppositely, it did not significantly affect the foam height after 10 minutes for the TX100-NB set. The effect of the presence of NB was assessed for each concentration. The p-values are gathered in **Table S6**. Those results demonstrated that the presence of nanobubbles in TX100 solutions did not significantly influence the foam evolution 10 minutes after its generation by microfluidics.

To summarise, further investigation with larger foam volumes, other ranges of liquid fraction and bubble size is required to better determine the real impact of the nanobubbles on the foam aging mechanisms.

6/ Summary & Perspectives

Up to now, few studies had been undertaken to determine if nanobubbles could affect dispersed systems such as foams or emulsions. This work introduced an original multi-scale, controlled, and systematic study of the effect of bulk nanobubbles on aqueous foams generated by microfluidics for two different surfactants over a broad range of concentrations.

Taking together all the dimensions at stake, those results first show that nanobubbles presented a limited effect on SDS solutions: for the exact same foaming process, similar interfacial properties resulted in the generation of high-quality foams for the whole range of concentration. However, the theoretical implications of these findings are unclear – notably, towards some effects of nanobubbles especially on the zeta potential and size of nanobubbles evolution induced by the foaming process at the lowest SDS concentration.

For the TX100 solutions, the increase in concentration improved the foaming efficiency, shifting from a very unstable foam to a stable one. It was shown here that the presence of nanobubbles in solution significantly impacted the foam quality at low and intermediate concentrations: the transition from poor-to-good foaming was shifted towards lower concentrations once NBs were added. Thus, the results of this research support the idea that nanobubbles can have an impact on foams made of microbubbles, and this effect is more evident at low and intermediate surfactant concentrations where NBs enhanced the foamability. Such findings need to be corroborated with other chemical systems, focusing on concentrations corresponding to the transition from poor to good foaming.

Regarding the mechanisms by which NB are acting on foaming, various scenarios can be proposed: on one hand, nanobubbles could act as particles and stabilize the foam by adsorbing at the interface. On the other hand, NB could help release large amounts of surfactant when adsorbing at gas-liquid interface, thus acting as surfactant reservoirs. Furthermore, NB could have a bulk effect, possibly preventing two microbubbles from coalescing. The adsorption of negatively charged nanobubbles at the foam gas-liquid interface could also increase the electrostatic repulsion between the two interfaces and prevent them from getting in contact and breaking. More experiments at the scale of single thin films are required to unravel the mechanisms by which NBs play a role in foamability.

From a practical point of view, these results suggest that processing effects can be important: a pre-foaming process (shaking, gas incorporation, etc.) could provide the generation of NBs within the solution, and could have an impact on the final foaming process. For example, a surfactant solution which is first “nanobubbled” (i.e, gas is injected to create NBs) could have different properties than the same solution without nanobubbles. Thereby, nanobubbles need to be considered when comparing chemical systems. The uncontrolled presence of nanobubbles, unintentionally included in the process, could play a non-expected role in the foaming properties. Oppositely, nanobubbles could be intentionally employed to reduce the concentration of stabilizers in foamed food products or cosmetics, thus reducing production costs, decreasing the quantity of fat or synthetic compounds employed in formulations, and their impact on the environment. Although this study focuses on foams, the findings may well have a bearing on other colloidal systems such as emulsions and nanoparticle dispersions.

ACKNOWLEDGEMENTS

This work was partially supported by the Engineering and Physical Sciences Research Council (grant number EP/R004382/1).

REFERENCES

[1] A. Saint-Jalmes, D. Langevin, Time evolution of aqueous foams: drainage and coarsening, J. Phys. Condens. Matter. 14 (2002) 9397. http://stacks.iop.org/0953-8984/14/i=40/a=325.

[2] A. Saint-Jalmes, Physical chemistry in foam drainage and coarsening, Soft Matter. 2 (2006) 836–849. https://doi.org/10.1039/B606780H.

[3] E.D. Manev, A. V Nguyen, Effects of surfactant adsorption and surface forces on thinning and rupture of foam liquid films, Int. J. Miner. Process. 77 (2005) 1–45. https://doi.org/https://doi.org/10.1016/j.minpro.2005.01.003.

[4] T.N. Hunter, R.J. Pugh, G. V Franks, G.J. Jameson, The role of particles in stabilising foams and emulsions, Adv. Colloid Interface Sci. 137 (2008) 57–81. https://doi.org/https://doi.org/10.1016/j.cis.2007.07.007.

[5] B.P. Binks, T.S. Horozov, Aqueous Foams Stabilized Solely by Silica Nanoparticles, Angew. Chemie Int. Ed. 44 (2005) 3722–3725. https://doi.org/10.1002/anie.200462470.

[6] R. Petkova, S. Tcholakova, N.D. Denkov, Foaming and Foam Stability for Mixed Polymer–Surfactant Solutions: Effects of Surfactant Type and Polymer Charge, Langmuir. 28 (2012) 4996–5009. https://doi.org/10.1021/la3003096.

[7] Z.A. AlYousef, M.A. Almobarky, D.S. Schechter, The effect of nanoparticle aggregation on surfactant foam stability, J. Colloid Interface Sci. 511 (2018) 365–373. https://doi.org/https://doi.org/10.1016/j.jcis.2017.09.051.

[8] F. Guo, S. Aryana, An experimental investigation of nanoparticle-stabilized CO2 foam used in enhanced oil recovery, Fuel. 186 (2016) 430–442. https://doi.org/10.1016/j.fuel.2016.08.058.

[9] N. Yekeen, M.A. Manan, A.K. Idris, E. Padmanabhan, R. Junin, A.M. Samin, A.O. Gbadamosi, I. Oguamah, A comprehensive review of experimental studies of

nanoparticles-stabilized foam for enhanced oil recovery, J. Pet. Sci. Eng. 164 (2018) 43–74. https://doi.org/https://doi.org/10.1016/j.petrol.2018.01.035.

[10] P. Nguyen, H. Fadaei, D. Sinton, Pore-Scale Assessment of Nanoparticle-Stabilized CO2 Foam for Enhanced Oil Recovery, Energy & Fuels. 28 (2014) 6221–6227. https://doi.org/10.1021/ef5011995.

[11] S. Andrieux, W. Drenckhan, C. Stubenrauch, Highly ordered biobased scaffolds: From liquid to solid foams, Polymer (Guildf). 126 (2017) 425–431. https://doi.org/10.1016/j.polymer.2017.04.031.

[12] S. Andrieux, W. Drenckhan, C. Stubenrauch, Generation of Solid Foams with Controlled Polydispersity Using Microfluidics, Langmuir. (2018). https://doi.org/10.1021/acs.langmuir.7b03602.

[13] J.R.T. Seddon, D. Lohse, W.A. Ducker, V.S.J. Craig, A Deliberation on Nanobubbles at Surfaces and in Bulk, ChemPhysChem. 13 (2012) 2179–2187. https://doi.org/10.1002/cphc.201100900.

[14] S.H. Oh, J.-M. Kim, Generation and Stability of Bulk Nanobubbles, Langmuir. (2017). https://doi.org/10.1021/acs.langmuir.7b00510.

[15] V.S.J. Craig, M.P. Krafft, Editorial overviewHot Topic - Nanobubbles and NanodropletsNanobubbles and Nanodroplets: from Basics to Applications, Curr. Opin. Colloid Interface Sci. 55 (2021) 101516. https://doi.org/https://doi.org/10.1016/j.cocis.2021.101516.

[16] M. Alheshibri, J. Qian, M. Jehannin, V.S.J. Craig, A History of Nanobubbles, Langmuir. 32 (2016) 11086–11100. https://doi.org/10.1021/acs.langmuir.6b02489.

[17] G. Liu, Z. Wu, V.S.J. Craig, Cleaning of protein-coated surfaces using nanobubbles: An investigation using a Quartz Crystal Microbalance, J. Phys. Chem. C. 112 (2008) 16748–

16753. https://doi.org/10.1021/jp805143c.

[18] H. Chen, H. Mao, L. Wu, J. Zhang, Y. Dong, Z. Wu, J. Hu, Defouling and cleaning using nanobubbles on stainless steel, Biofouling. 25 (2009) 353–357. https://doi.org/10.1080/08927010902807645.

[19] M. Fan, D. Tao, R. Honaker, Z. Luo, Nanobubble generation and its application in froth flotation (part I): nanobubble generation and its effects on properties of microbubble and millimeter scale bubble solutions, Min. Sci. Technol. 20 (2010) 1–19. https://doi.org/https://doi.org/10.1016/S1674-5264(09)60154-X.

[20] M. Fan, D. Tao, R. Honaker, Z. Luo, Nanobubble generation and its applications in froth flotation (part II): fundamental study and theoretical analysis, Min. Sci. Technol. 20 (2010) 159–177. https://doi.org/https://doi.org/10.1016/S1674-5264(09)60179-4.

[21] N. Nirmalkar, A.W. Pacek, M. Barigou, Interpreting the interfacial and colloidal stability of bulk nanobubbles, Soft Matter. 14 (2018) 9643–9656. https://doi.org/10.1039/C8SM01949E.

[22] J.H. Weijs, J.R.T. Seddon, D. Lohse, Diffusive Shielding Stabilizes Bulk Nanobubble Clusters, ChemPhysChem. 13 (2012) 2197–2204. https://doi.org/10.1002/cphc.201100807.

[23] A. Ushida, T. Hasegawa, N. Takahashi, T. Nakajima, S. Murao, T. Narumi, H. Uchiyama, Effect of mixed nanobubble and microbubble liquids on the washing rate of cloth in an alternating flow, J. Surfactants Deterg. 15 (2012) 695–702. https://doi.org/10.1007/s11743-012-1348-x.

[24] K. Yasui, T. Tuziuti, N. Izu, W. Kanematsu, Is surface tension reduced by nanobubbles (ultrafine bubbles) generated by cavitation?, Ultrason. Sonochem. (2018). https://doi.org/https://doi.org/10.1016/j.ultsonch.2018.11.020.

[25] M. Zhang, J.R.T. Seddon, Nanobubble–Nanoparticle Interactions in Bulk Solutions,

Langmuir. 32 (2016) 11280–11286. https://doi.org/10.1021/acs.langmuir.6b02419.

[26] M. Zhang, J.R.T. Seddon, S.G. Lemay, Nanoparticle–nanobubble interactions: Charge inversion and re-entrant condensation of amidine latex nanoparticles driven by bulk nanobubbles, J. Colloid Interface Sci. 538 (2019) 605–610. https://doi.org/10.1016/j.jcis.2018.11.110.

[27] D. Tao, A. Sobhy, L. Li, Nanobubble effects on hydrodynamic interactions between particles and bubbles, Powder Technol. (2019). https://doi.org/https://doi.org/10.1016/j.powtec.2019.02.024.

[28] A. Sobhy, D. Tao, Effects of Nanobubbles on Froth Stability in Flotation Column, Int. J. Coal Prep. Util. 39 (2019) 183–198. https://doi.org/10.1080/19392699.2018.1459582.

[29] S. Calgaroto, A. Azevedo, J. Rubio, Flotation of quartz particles assisted by nanobubbles, Int. J. Miner. Process. 137 (2015) 64–70. https://doi.org/https://doi.org/10.1016/j.minpro.2015.02.010.

[30] S. Nazari, S.Z. Shafaei, M. Gharabaghi, R. Ahmadi, B. Shahbazi, Effect of frother type and operational parameters on nano bubble flotation of quartz coarse particles, J. Min. Environ. 9 (2018) 539–546. https://doi.org/10.22044/jme.2017.6404.1461.

[31] D. Vigolo, S. Buzzaccaro, R. Piazza, Thermophoresis and thermoelectricity in surfactant solutions., Langmuir. 26 (2010) 7792–7801. https://doi.org/10.1021/la904588s.

[32] N.M. Kovalchuk, M. Sagisaka, K. Steponavicius, D. Vigolo, M.J.H. Simmons, Drop formation in microfluidic cross-junction: jetting to dripping to jetting transition, Microfluid. Nanofluidics. 23 (2019) 103. https://doi.org/10.1007/s10404-019-2269-z.

[33] C. Thévenot, B. Grassl, G. Bastiat, W. Binana, Aggregation number and critical micellar concentration of surfactant determined by time-dependent static light scattering (TDSLS) and conductivity, Colloids Surfaces A Physicochem. Eng. Asp. 252 (2005) 105–111.

https://doi.org/https://doi.org/10.1016/j.colsurfa.2004.10.062.

[34] P. Kim, K.W. Kwon, M.C. Park, S.H. Lee, S.M. Kim, K.Y. Suh, Soft Lithography for Microfluidics: a Review, BIiochip J. 2 (2008) 1–11. internal-pdf://0720923336/soft lithography description.pdf.

[35] L. Labarre, D. Vigolo, Microfluidics approach to investigate foam hysteretic behaviour, Microfluid. Nanofluidics. 23 (2019) 129. https://doi.org/10.1007/s10404-019-2299-6.

[36] A.E. Mark, A.J. Michael, K.G. Bruce, Determining the optimal PDMS–PDMS bonding technique for microfluidic devices, J. Micromechanics Microengineering. 18 (2008) 67001. http://stacks.iop.org/0960-1317/18/i=6/a=067001.

[37] T. Cubaud, U. Ulmanella, C.-M. Ho, Two-phase flow in microchannels with surface modifications, Fluid Dyn. Res. 38 (2006) 772–786. https://doi.org/http://dx.doi.org/10.1016/j.fluiddyn.2005.12.004.

[38] W.A.C. Bauer, M. Fischlechner, C. Abell, W.T.S. Huck, Hydrophilic PDMS microchannels for high-throughput formation of oil-in-water microdroplets and water-in-oil-in-water double emulsions, Lab a Chip - Miniaturisation Chem. Biol. 10 (2010) 1814–1819. https://doi.org/10.1039/c004046k.

[39] S.A. Peyman, R.H. Abou-Saleh, J.R. McLaughlan, N. Ingram, B.R.G. Johnson, K. Critchley, S. Freear, J.A. Evans, A.F. Markham, P.L. Coletta, S.D. Evans, Expanding 3D geometry for enhanced on-chip microbubble production and single step formation of liposome modified microbubbles, Lab Chip. 12 (2012) 4544–4552. https://doi.org/10.1039/C2LC40634A.

[40] S.A. Peyman, J.R. McLaughlan, R.H. Abou-Saleh, G. Marston, B.R.G. Johnson, S. Freear, P.L. Coletta, A.F. Markham, S.D. Evans, On-chip preparation of nanoscale contrast agents towards high-resolution ultrasound imaging, Lab Chip. 16 (2016) 679–687.

https://doi.org/10.1039/C5LC01394A.

[41] L.L. Schramm, Emulsions, Foams, and Suspensions: Fundamentals and Applications, Wiley-VCH Verlag GmbH & Co. KGaA, Weinheim, 2006. https://doi.org/10.1002/3527606750.

[42] E. Nowak, Z. Xie, N.M. Kovalchuk, O.K. Matar, M.J.H. Simmons, Bulk advection and interfacial flows in the binary coalescence of surfactant-laden and surfactant-free drops, Soft Matter. 13 (2017) 4616–4628. https://doi.org/10.1039/C7SM00328E.

[43] N. Nirmalkar, A.W. Pacek, M. Barigou, On the Existence and Stability of Bulk Nanobubbles, Langmuir. 34 (2018) 10964–10973. https://doi.org/10.1021/acs.langmuir.8b01163.

[44] N. Nirmalkar, A.W. Pacek, M. Barigou, Interpreting the interfacial and colloidal stability of bulk nanobubbles, Soft Matter. (2018). https://doi.org/10.1039/C8SM01949E.

[45] J. Il Lee, J.-M. Kim, Role of anionic surfactant in the generation of bulk nanobubbles by ultrasonication, Colloid Interface Sci. Commun. 46 (2022) 100578.

[46] B. Janczuk, J.M. Bruque, M.L. Gonzalez-Martin, C. Dorado-Calasanz, The Adsorption of Triton X-100 at the Air-Aqueous Solution Interface, Langmuir. 11 (1995) 4515–4518. https://doi.org/10.1021/la00011a055.

[47] J. Eastoe, J.S. Dalton, Dynamic surface tension and adsorption mechanisms of surfactants at the air–water interface, Adv. Colloid Interface Sci. 85 (2000) 103–144. https://doi.org/http://dx.doi.org/10.1016/S0001-8686(99)00017-2.